Indian Journal of Biochemistry & Biophysics
Vol. 62, April 2025, pp. 406-425
DOI: 10.56042/ijbb.v62i4.14277

Spectroscopic study, Quantum Chemical Investigations, *In silico* and Drug Likeness of 4-Chloro-6,7-dimethoxyquinazoline: A potent study of new anti-alzheimer agent

Karthikeyan Asokan, Sumathi Sivaraman, Karthik Nallasamy, Jeyavijayan Subbiah & Selvarengan Paranthaman**

Department of Physics, Kalasalingam Academy of Research and Education (Deemed to be University), Krishnankoil-626 126, Tamil Nadu, India

Received 09 October 2024; revised 14 November 2024

Alzheimer's disease (AD) is one of the most severe illnesses linked to aging. The present work examined the potential of 4-Chloro-6,7-dimethoxyquinazoline (CDQ) as anti-alzheimer drug using spectroscopic (FT-IR, FT-Raman, and UV-Vis) and computational techniques. The molecular geometries of CDQ were optimized using DFT/B3LYP/6-311++G(d,p). The calculation of vibrational frequencies is based on the potential energy distribution (PED). The calculated frequencies using DFT matches well with the experimental values. Time-dependent density functional theory (TD-DFT) have been used to study the frontier molecular orbitals (FMO) in order to determine the energy gap, global reactive parameters, and other related molecular features. The molecular electrostatic potential (MEP) and the mulliken charge analysis determine the regions that are most susceptible to electrophilic and nucleophilic attacks. The charge delocalization and stability of the studied molecule were examined using Natural Bond Orbital (NBO) analysis. Multiwfn software had been employed to perform the topological studies of LOL, RDG, NCI, and ELF. In order to validate the biological activity, molecular docking studies were carried out to stimulate the binding orientation and affinity of CDQ against four AChE proteins. According to our docking analysis, CDQ and the 4EY7 protein have a significant interaction, with a binding energy of -7.5 kcal mol^{-1}. In addition, the stability of the protein-ligand interaction had been assessed using molecular dynamics simulations. Studies on the ADMET prediction of CDQ have also been carried out. These findings provide a very interesting and feasible details regarding the title compound for potential future investigation.

Keywords: 4-chloro-6,7-dimethoxyquinazoline, ADMET properties, Alzheimer's disease, DFT, Molecular docking, Molecular dynamics

Alzheimer's disease (AD) is a progressive long-term neurodegenerative condition that affects brain illness memory, thinking, and performance in regular life[1].Based on data from the World Health Organisation (WHO), the number of persons affected by dementia is estimated to be 55 million worldwide, and will increase to 78 million in 2030 and 139 million by 2050[2]. Certainly, AD is a significant and expanding global issue, the development of novel and efficient therapies for AD treatment is an essential area of pharmaceutical research[3]. Many hypotheses have been offered to explain the causes of AD, including amyloid β (Aβ)[4], Tau[5], cholinergic neuron damage[6], oxidative stress[7], inflammation, and others. At now, the cholinergic hypothesis serves as the foundation for the majority of AD treatment.This hypothesis proposes that cholinergic neurons are degraded and acetylcholine (ACh) is rapidly hydrolyzed by cholinesterases.Human brains have two cholinesterases: Acetylcholinesterase (AChE) and butyrylcholinesterase (BChE) are enzymes that break down ACh. Inhibiting these cholinesterases can aid in the treatment of AD by preventing the hydrolysis of ACh[8]. AChE is the primary neurotransmitter in the peripheral and central nervous systems, found at the synapse between nerve and muscle cells[9]. Its primary biological function is to quickly hydrolyze ACh to stop neurotransmission.Cholinergic neuro-transmission defects are critical for AD progression. Through cholinergic pathways, it makes a major contribution to brain function. AChE has been extensively studied in tissues relevant to AD since the identification of cholinergic deficiency. AChE inhibition is the most effective therapeutic target for treating AD symptoms[10]. The FDA has approved four cholinesterase inhibitors for AD treatment, including galantamine, donepezil, rivastigmine, and tacrine.But

*Correspondence:
E-mail: psrengan@hotmail.com
Suppl. Data available on respective page of NOPR

these drugs are only slightly helpful in treating symptoms[11]. Long-term clinical use indicates that these drugs are only palliative treatments and do not address essential biological processes. Because AD is a multifactorial illness with variability and complexity, developing drugs for its treatment is difficult[12]. In addition to the drug's potential, blood-brain barrier (BBB) permeability is an important consideration in the development of drugs targeting the central nervous system (CNS). Thus, the current focus is on developing novel cholinesterase inhibitors to treat AD more successfully.

Quinazoline derivatives, which are classified as N-containing heterocyclic compounds, have raised concerns across all regions because of their diverse and widely-reaching biological activity[13]. Due to their low toxicity, quinazoline pharmacophore units are found in many approved drugs. That are regarded to be an appropriate starting point for the development of novel therapeutic compounds for various kinds of disorders.The quinazoline ring has multiple locations that can be substituted, but the 2-, 4-, and 6-positions are thought to be the main pharmacophoric sites for enhancing biological activities[14]. Figure 1A shows the quinazoline drug, and (Fig. 1B) shows the 4-Chloro-6,7-dimethoxyquinazoline (CDQ). The 2, 4 and 6th positions has H, H and methyl group (CH_3) in CDQ shows good biological responses. For this purpose, we had chosen quinazoline (CDQ) derivatives for AD treatment.Using newly developed synthetic techniques, medicinal chemists synthesised a variety of quinazoline compounds with varied biological activity by attaching different active groups to the quinazoline molecule. Additionally, research has been done on the quinazoline derivatives possible uses in the areas of biology, pesticides, and medicine. Numerous medicinal properties of quinazoline derivatives have already been identified by researchers. That includes anti-bacterial[15],anti-cancer[16],anti-oxidation[17], anti-malarial[18], anti-obesity[19], anti-psychotic[20], and anti-diabetes[21]*etc*. Recently, quinazoline derivatives received great attention for the AD treatment. After a literature search it has been suggested that quinazoline derivatives may be useful for a variety of treatments related to AD.

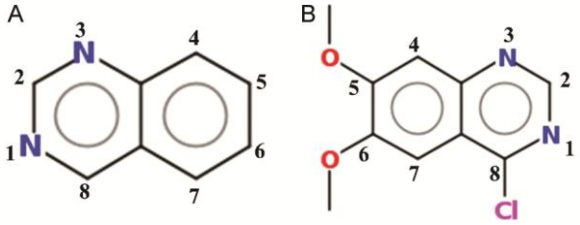

Fig. 1 — (A) Quinazoline drug; and (B) 4-chloro-6, 7-dimethoxyquinazoline

As of right now, no research has been done on the4-Chloro-6,7-dimethoxyquinazoline (CDQ) molecule as a possible Alzheimer's drug. Consequently, in this work we have examined the biological activity of CDQmore especially, its anti-Alzheimer activity using both theoretical and experimental methods. Research is done on the spectroscopic investigations, pharmacodynamic properties, and toxicological characteristics. Through molecular docking studies, the protein-ligand interaction and binding affinity were investigated. Molecular dynamics simulations were used to evaluate protein-ligand complexes in order to confirm their stability. Density functional theory (DFT) calculations in the B3LYP/6-311++G(d,p) basis set can be utilised to explain the fundamental properties of numerous molecules, making this a cost-effective and feasible approach. The energy difference between the highest occupied and lowest unoccupied orbitals have been utilised to calculate the molecule's chemical reactivity, structural stability, and Frontier molecular orbital (FMO). The mapped surface has been employed to calculate the MEP, which confirms the molecule's reactivity.

Experiment and Computational details

Experimental Study

A 4-Chloro-6,7-dimethoxyquinazoline(CDQ) powder sample with over 98% purity were obtained from Sigma Aldrich Co, in India and used directly for spectrum measurements.Perkin Elmer's two-FT-IR/ATR spectrometer system has a scan rate of 25 and a resolution of 4 cm^{-1} within the wavenumber range of 4000 to 400 cm^{-1}. The Fourier Transform Infrared (FT-IR) spectrum was recorded in the mid-IR region using the KBr pellet technique. A Bruker RFS 27 Stand-alone spectrometer system with 1 cm^{-1}resolution have been used to record the FT-Raman spectrum in the mid-IR region. The 1064 nm line of Nd: YAG laser was used for excitation at 100 mW power. UV-A Shimadzu 1700 spectrometer was used to analyze the UV-Vis spectrum of a water solution in the range of 250 to 400 nm.

DFT calculations

A computational modelling approach, known as DFT, have been employed to study the electronic

structure of selected systems. All computations were performed using the higher-order basis set B3LYP/6-311++G(d,p) for both gas phase and water environments, utilizing the Gaussian 09 software version[22]. The analysis of bond lengths and bond angles, along with molecular geometries, have been analysed. Vibrational wavenumbers were assigned using potential energy distribution values using Vibrational Energy Distribution Analysis (VEDA 4) program. Charge transfers within the molecule, in each phase, were explained through HOMO-LUMO analysis. Intramolecular interactions and charge transfers were further explored using Mulliken and NBO analysis. The GaussView program[23]has been employed to plot the FMO, which contained a MEP map and an energy distribution from HOMO to LUMO. The computed values are compared with experimental data in order to assess the computational method's efficiency.

Topology studies

The ELF (Electron Localisation Function) could help us to understand how electrons are distributed within a molecule or material. This real-space function evaluates the extent of electronic charge density localization within a system. The LOL (Localized Orbital Locator) is useful for studying chemical bonds in molecules, indicating the atoms that are involved and the degree of orbital overlap. It is capable of predicting the reactivity of a molecule and identify the lone pairs of electrons. The ELF and LOL were estimated using quantum mechanical methods such as DFT. A three-dimensional map is often used to represent electron distribution in space. The Multiwfn application generates maps with shaded surfaces that show orbital locators and electron localisation[24].

Molecular Docking

Molecular docking is an important computational approach for drug discovery. This method uses three-dimensional structures to predict how ligands (small molecules) will interact with receptors (macromolecules) in their active sites[25]. From the Pubchem database the experimental geometry of CDQ (Pubchem ID:2769364) have been obtained. Before starting docking studies, the structure of CDQ had been optimised using B3LYP with the 6-311++G (d,p) basis set. Through the RCSB Protein Data Bank (http://www.rcsb.org/pdb/), the target proteins have been retrieved. The CDQ (ligand) is docked against four target AChE proteins: 4EY7, 1EVE, 4PQE and 3I6M. The standard cleaning procedures had been completed before the docking was performed. Proteins were prepared using Biovia Discovery Studio[26] by adding charges and polar hydrogen atoms at the same time removing cofactors, water molecules, and metal ions. Following the preparation process, the proteins have been moved to PyRx and converted into macromolecules. The ligand is converted to PDB format before being entered into PyRx's Auto Dock Vina. At last, PDBQT had been generated for the proteins and ligands, and they're now ready for docking. Protein-ligand docking was carried out using PyRx 0.8 (https://pyrx.sourceforge.io/) software[27].

Molecular dynamics

Molecular dynamics (MD) simulation is a more accurate computational technique. Moreover, it performs better than the docking method, which requires less computing power. With extreme precision, it generates results that may not be achievable with experimental methods, but can offer insight into the behaviour of complicated systems. Protein-ligand complex stability is commonly investigated using MD modelling. In this calculation, the GROMOS 96 force field was employed for simulation, and the GROMACS 4.6.3 package were used. The mobility of molecules and atoms in MD simulations has been calculated. Utilising the findings of the studies on the RMSD (Root Mean Square Deviation), RMSF (Root Mean Square Fluctuation), radius of gyration, hydrogen bond, and other relevant factors, simulation was performed.

ADMET and physicochemical properties

The compound must be validated by a variety of characteristics before they can be classified as therapeutic molecules, including ADMET features, physicochemical qualities, and toxicity. We validated our molecule with several bioinformatics tools. pkCSM (https://biosig.lab.uq.edu.au/pkcsm/) is a free *in silico* online program that predicts ADMET features using graph-based signatures to create predictive models. An independent SMILES string or a SMILES file with a header can be entered as input format for predicting ADMET. Drug design and clinical success depend on ADMET characteristics. Early ADMET characteristic prediction reduced compound failure rates for future process. One of the most popular online sources for quickly predicting physicochemical parameters is SwissADME (www.swissadme.ch). Other parameters such as drug likeness, lipophilicity and water solubility have also

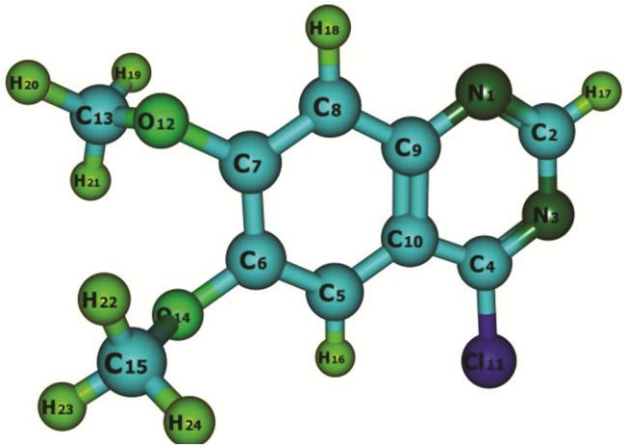

Fig. 2 — Optimized 3d structure of 4-chloro-6,7-dimethoxyquinazoline

been calculated. Additionally, the relationship between the compound's physicochemical characteristics and molecular activity is assessed using molinspiration, an open-access web server (https://www.molinspiration.com/cgi-bin/properties).

Results and Discussion

Structural parameters

The optimized 3d molecular structure of CDQ with atom's numbering is shown in (Fig. 2). The theoretical bond lengths and bond angles with the XRD values[28] are shown in (Table 1). Global minimum energies of the title compound under study are -1106.80422 Hartree for gas phase and -1106.81303 Hartree for water, respectively and it is symmetric in the C1 point group. Using the DFT/B3LYP approach, the optimized structural parameters of CDQ have been done with the 6-311++G(d,p) basis set in both the gas phase and the water as shown in (Table 1). The theoretically estimated bond lengths and bond angles have been slightly contrasted to published XRD data. Since the CDQ is theoretically calculated in the gas phase, whereas the experimental component was done in the solid phase. The title compound structure is composed of seven C-C interactions, four C-N, four C-O, one C-Cl, and nine C-H links. By using above technique, the enlarged C-C bond distances of 1.37 to 1.43 Å are in good agreement with the reported experimental XRD (1.35-1.45Å). The bond lengths of C4–Cl11 are greater than the bond distances of CDQ. This is in agreement with the experimental value of 1.76 Å. Thus, it is evident that the π-electrons around these bonds have not gone through any delocalisation.

Table 1 — The optimized structural parameters of 4-Chloro-6,7-dimethoxyquinazoline

Structural parameters			
Bond length (Å)	DFT-B3LYP/6-311++G(d,p)		Experimental[28]
	In gas phase	In water	
N1-C2	1.31	1.31	1.30
N1-C9	1.36	1.37	1.39
C2-N3	1.36	1.36	1.33
C2-H17	1.09	1.08	-
N3-C4	1.30	1.30	1.34
C4-C10	1.42	1.42	1.45
C4-Cl11	1.76	1.76	-
C5-C6	1.37	1.37	1.35
C5-C10	1.41	1.41	1.42
C5-H16	1.08	1.08	0.93
C6-C7	1.43	1.43	1.43
C6-O14	1.37	1.37	1.37
C7-C8	1.37	1.38	1.39
C7-O12	1.37	1.36	1.35
C8-C9	1.41	1.41	1.39
C8-H18	1.08	1.08	0.93
C9-C10	1.43	1.43	1.39
O12-C13	1.44	1.45	1.42
C13-H19	1.09	1.09	0.96
C13-H20	1.09	1.09	0.96
C13-H21	1.09	1.09	0.96
O14-C15	1.44	1.44	1.42
C15-H22	1.09	1.09	0.96
C15-H23	1.09	1.09	0.96
C15-H24	1.09	1.09	0.96
	Bond angle (°)		
C2-N1-C9	116.6	116.9	113.9
N1-C2-N3	126.9	126.7	131.6
N1-C2-H17	117.7	117.9	-
N3-C2-H17	115.4	115.5	-
C2-N3-C4	116.6	116.6	115.4
N3-C4-C10	123.9	124.1	120.3
N3-C4-Cl11	116.7	116.4	-
C10-C4-Cl11	119.4	119.5	-
C6-C5-C10	120.3	120.4	122.0
C6-C5-H16	119.1	119.0	119.0
C10-C5-H16	120.6	120.6	119.0
C5-C6-C7	120.1	120.1	120.0
C5-C6-O14	119.7	119.5	125.0
C7-C6-O14	120.1	120.4	114.4
C6-C7-C8	120.2	120.2	119.0
C6-C7-O12	120.1	120.5	116.0
C8-C7-O12	119.6	119.2	125.0
C7-C8-C9	120.6	120.7	120.0
C7-C8-H18	120.3	119.9	120.0
C9-C8-H18	119.1	119.4	120.0
N1-C9-C8	119.3	119.5	118.0

(*Contd*.)

(*Contd*.)

N1-C9-C10	121.7	121.6	120.0
C8-C9-C10	119.0	119.0	122.0
C4-C10-C5	126.1	126.0	126.0
C4-C10-C9	114.2	114.2	116.0
C5-C10-C9	119.7	119.7	117.0
C7-O12-C13	115.6	116.2	118.2
O12-C13-H19	110.1	109.8	110.0
O12-C13-H20	105.9	105.8	110.0
O12-C13-H21	111.2	111.0	109.0
C19-C13-H20	109.5	109.8	109.0
C19-C13-H21	110.1	110.3	109.0
C20-C13-H21	110.0	110.0	109.0
C6-O14-C15	115.3	115.5	116.3
O14-C15-H22	111.1	110.9	109.0
O14-C15-H23	106.0	105.9	109.0
O14-C15-H24	110.2	110.0	109.0
H22-C15-H23	110.0	109.9	109.0
H22-C15-H24	110.0	110.2	109.0
H23-C15-H24	109.5	109.8	109.0

The title compound N1-C2, N1-C9, N3-C4, C2-N3, and C6-O14, C7-O12, O12-C13, and O14-C15 has bond lengths of 1.31 Å, 1.36 Å, 1.30 Å, 1.36 Å and 1.37 Å, 1.37 Å, 1.44 Å, 1.44 Å as determined using the DFT. These results show a good agreement with the 1.30 Å, 1.39 Å, 1.34 Å, 1.33 Å and 1.37 Å, 1.35 Å, 1.42 Å, and 1.42Å experimental values. Since the bond angles increase with increasing atom electronegativity. The C6-C5-C10 has a computed bond angle of 120.3 Å and experimental by 122.0 Å,which is larger than other C–C–C angles. The estimated bond angles of C6–C7–O12 and C5–C6–O14 are 120.1 Å and 119.7 Å, respectively. Which has good agreement with experimental values of 116.0 Å and 125.0 Å and the oxygen atom linked at C6 and C7. With experimental data, the gas phase and water are well matched, and the atoms of the CH_3 methyl groups are connected at O12 and O14.

Thermodynamic parameters

Thermodynamic parameters are important for understanding and designing chemical processes. All computations are based on the assumption that the contributions from translation, rotation, and electronic motion are within the ideal gas approximation[29]. The thermodynamic parameters of CDQ were calculated using DFT/B3LYP/6-311++G(d,p) basis set for gas phase and water. These values include heat capacity, entropy, and zero-point energy as shown in (Table 2). The CDQ molecule has a total dipole moment of 3.961 Debye for gas phase and 5.290 Debye for water. The larger dipole moment indicates strong bond exists between the atoms of CDQ molecule. Due to this high polar nature, CDQ shows high stability in the water. The simulations show that the zero-point vibrational energy (ZPVEs) vary greatly, from 111.411 kcal mol^{-1} for gas phase to 111.174 kcal mol^{-1} for water. The total entropy (s) 116.371 cal $mol^{-1}K^{-1}$ for gas phase and for water 117.400 cal $mol^{-1}K^{-1}$. The information drawn from the above-mentioned thermodynamic parameters (S, Cp, and H) could be useful in determining alternative thermodynamic energy relationships. The use of thermodynamic function relationships simplifies the estimation of additional energy and aids in the synthesis of related chemicals for future research. The thermodynamic parameters of CDQ are given in (Table 2).

Table 2 — The thermodynamic parameters of 4-Chloro-6, 7-dimethoxyquinazoline

Parameters	DFT-B3LYP/6-311++G(d,p)	
	In gas phase	In water
Optimized global minimum Energy (Hartrees)	-1106.80422	-1106.81303
Total energy(thermal), E_{total}(kcal mol^{-1})	119.864	119.702
Heat capacity, C_v (cal $mol^{-1}K^{-1}$)	49.612	49.797
Total Entropy, S (cal $mol^{-1}K^{-1}$)	116.371	117.400
Translational Entropy (cal $mol^{-1}K^{-1}$)	42.122	42.122
Rotational Entropy (cal $mol^{-1}K^{-1}$)	32.497	32.500
Vibrational Entropy (cal $mol^{-1}K^{-1}$)	41.751	42.777
Vibrational energy, E_{vib} (kcal mol^{-1})	118.087	117.925
Zero-point vibrational energy, (kcal mol^{-1})	111.411	111.174
Rotational constants (GHz)		
A	0.945	0.946
B	0.363	0.362
C	0.275	0.274
Dipole moment (Debye)	3.961	5.290

Vibrational assignments

There are 24 atoms in all in the complex structure known as CDQ, that contains 132 electron and 66 vibrational modes through 3N–6. Figures 3 and 4 shows the theoretical FT-IR and FT-Raman spectrum related to the experimental data. Table 3 presents the vibrational assignments (calculated infrared intensities, scaled vibrational frequencies, and Raman intensity) based on potential energy distribution (PED) for CDQ. The VEDA software was utilized for vibrational assignments[30]. The vibrational frequencies were measured on the 0.9613 scale. There is a tiny

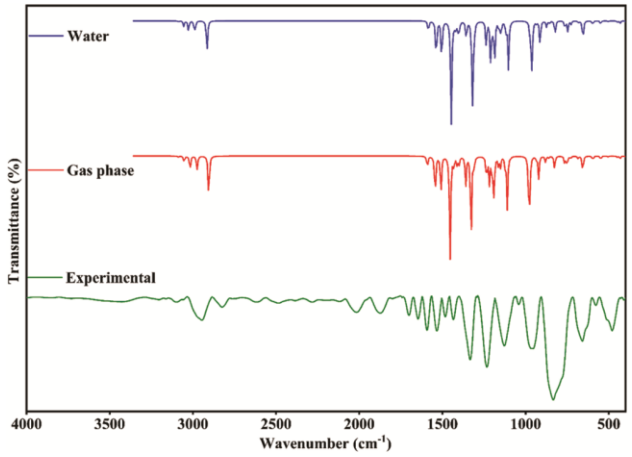

Fig. 3 — FT-IR spectrum of 4-Chloro-6,7-dimethoxyquinazoline

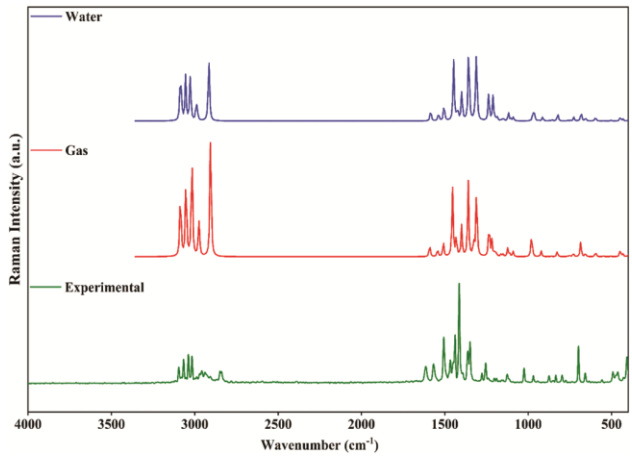

Fig. 4 — FT-Raman spectrum of 4-Chloro-6, 7-dimethoxyquinazoline

discrepancy between the two sets of data because theoretical wave numbers are obtained from the gaseous state, while the experimental wave numbers are derived from the solid state.

C-C, C–H, N-C and C-O vibrations

The range of the carbon-carbon stretching vibration is 1650–1100 cm^{-1}. At 1600, 1540, 1495, and 1445 cm^{-1} and at 1568, 1510, 1460, and 1448 cm^{-1}, the FT-IR spectrum and the FT-Raman spectrum had identical vibrations respectively. There is a theoretical range of 1590–1432 cm^{-1} for C–C stretching vibrations. As well as the PED contributions, which vary from 87% to 90%, this suggests a significant agreement between the experimental and theoretical results. In the region of 3100–3000 cm^{-1}, it was found that hetero aromatic compounds had C–H vibrations. Stretching vibrations of C–H have been observed experimentally at 3086 cm^{-1} in FT-IR and 3090, 3060 cm^{-1} in FT-Raman spectrum. In DFT, the frequencies at which this vibration should be detected with 99 and 100% PED are 3088, 3084, and 3052 cm^{-1}. The mixed band of the N–C vibration occurs between 1400 and 1200 cm^{-1}. N–C vibrations have been detected at 1335 and 1241 cm^{-1} and 1362 and 1300 cm^{-1}, respectively, in the FT-IR and FT-Raman spectrum of the title molecule. The theoretical peak measurement falls between 1349 and 1224 cm^{-1}. In that sequence, PED accounts for 81, 80, 79, and 78% of the total. Between 1250 and 850 cm^{-1}, the CDQ pyrone ring's C-O stretching is located. The FT-Raman values that have been observed at 1210, 1195, 1180, and 1170 cm^{-1}. The matching DFT values are measured at 1218, 1201, 1190, and 1164 cm^{-1}. The CDQ carbonyl group's bending deformations are shown in (Table 3). Table 3 lists further in-plane and out-of-plane vibrations of C–C, C–H, N–C, and C–O bonds.

C–Cl vibrations

A halogen (Cl11) atom physically linked to a benzene ring, that often generates a broad range between 760 and 370 cm^{-1} because the C–Cl stretching vibrations tend to combine with ring vibration. For the C-Cl stretching vibration of CDQ, the FT-IR spectrum displays a very weak peak at 544 cm^{-1}. These wavenumbers intensity is fairly high, matching the levels predicted by computation at 548 cm^{-1} (52% PED). There is a strong correlation between PED values and other modes. Table 3 displays the C-Cl in-plane and out-of-plane modes for CDQ.

CH_3 vibrations

It is anticipated that the two O-CH_3 groups connected to the benzene ring's C6 and C7 places in the title molecule will produce a variety of bending and stretching vibrations. The following definition applies to the nine fundamental vibrations of the CH_3 groups: CH_3 ss stands for symmetric stretch; CH_3 ips for in-plane stretch (in-plane hydrogen stretching modes); CH_3 ipb for in-plane bending (hydrogen deformation modes); CH_3 sb for symmetric bending; CH3 ipr for in-plane rocking; CH_3 opr for out-of-plane rocking; CH_3 ops for out-of-plane stretch; CH_3 opb for out-of-plane bending modes; and tCH_3 for twisting modes. For the CH_3 group, the symmetric mode is estimated to be about 2870 cm^{-1}, while the asymmetric mode is projected to be 2980 cm^{-1}. The FT-Raman and FT-IR spectrum of CDQ show medium and weak intensity bands that are attributed to the two methyl groups' in-plane stretching vibrations. The recorded spectrum and the findings

Table 3 — The vibrational assignments based on Potential Energy Distrubution calculations for 4-Chloro-6,7-dimethoxyquinazoline

S. No	Observed wave number (cm^{-1})		Wavenumber (cm^{-1})		IR Intensity (Km mol^{-1})	Raman activity (Å^4 amu^{-1})	Assignment with PED (%)
	FT-IR	FT- Raman	Calculated	Scaled			
1	-	3090(ms)	3212	3088	2	73	νCH(100)
2	3086(vw)	-	3208	3084	0	73	νCH(98)
3	-	3060(ms)	3175	3052	16	190	νCH(99)
4	3028(vw)	-	3139	3018	19	126	CH_3ips(97)
5	-	3017(ms)	3138	3016	19	121	CH_3ips(95)
6	-	2974(vw)	3096	2976	20	47	CH_3ss(96)
7	-	2970(vw)	3092	2973	20	37	CH_3ss(94)
8	29025(ms)	-	3023	2906	54	182	CH_3ops(93)
9	2870(ms)	-	3021	2904	63	107	CH_3ops(92)
10	1600(w)	-	1655	1591	30	19	νCC(91)
11	1540(ms)	1568(ms)	1606	1544	114	11	νCC(89)
12	1495(ms)	1510(ms)	1570	1509	102	22	νCC(90)
13	-	1460(vw)	1513	1454	260	93	νCC(87)
14	-	1448(ms)	1508	1450	18	9	νCC(88)
15	1445(ms)	-	1505	1447	2	1	νCC(85)
16	-	1439(vw)	1491	1433	2	10	νCC(86)
17	-	1435(vw)	1490	1432	17	10	CH_3ipb(84)
18	-	1430(vw)	1486	1429	7	7	CH_3ipb(83)
19	-	1413(vw)	1468	1411	24	1	CH_3 sb (82)
20	-	1385(vw)	1456	1399	19	42	CH_3sb (80)
21	-	1362(vw)	1415	1360	75	105	νCN(81)
22	1335(s)	-	1381	1328	229	19	νCN(79)
23	-	1300(vw)	1363	1310	28	104	νCN(78)
24	1241(s)	-	1285	1235	60	47	νCN(77)
25	-	1210(vw)	1267	1218	69	21	νCO(75)
26	-	1195(vw)	1249	1201	58	8	νCO(76)
27	-	1180(vw)	1237	1190	108	3	νCO(74)
28	-	1170(vw)	1211	1164	21	3	νCO(73)
29	-	1152(vw)	1198	1152	30	3	CH_3opb(71)
30	1130(ms)	-	1169	1124	5	1	CH_3opb(72)
31	-	1120(vw)	1168	1122	21	11	CH_3opr(70)
32	-	1115(vw)	1155	1110	132	3	CH_3opr(69)
33	1062(vw)	-	1134	1090	2	7	bCH (68)
34	-	978(vw)	1022	982	76	19	bCH (67)
35	968(s)	-	1014	975	104	10	bCH (65)
36	-	924(vw)	974	936	7	0	CH_3 ipr(66)
37	-	919(vw)	959	922	57	7	CH_3ipr(64)
38	-	879(vw)	916	881	16	0	Rasymd(63)
39	854(vs)	-	896	861	4	1	Rsymd(62)
40	-	827(vw)	859	826	35	7	Rtrigd(61)
41	-	788(vw)	796	765	22	0	Rasymd(60)
42	-	745(vw)	781	751	24	2	Rsymd(59)
43	-	720(vw)	759	730	6	4	Rtrigd(58)
44	687(vw)	-	713	685	6	19	bCO(57)
45	-	655(ms)	683	657	43	4	bCO(55)
46	603(vw)	-	629	605	1	0	bCO(54)
47	-	585(vw)	619	595	10	6	bCO(53)
48	544(vw)	-	571	548	9	1	νCCl(52)
49	492(ms)	498(vw)	526	505	2	1	ωCH(56)
50	-	-	466	448	4	8	ωCH(51)

(*Contd*.)

Table 3 — The vibrational assignments based on Potential Energy Distrubution calculations for 4-Chloro-6, 7-dimethoxyquinazoline(*Contd*.)

S. No	Observed wave number (cm^{-1})		Wavenumber (cm^{-1})		IR Intensity (Km mol^{-1})	Raman activity ($Å^4$ amu^{-1})	Assignment with PED (%)
	FT-IR	FT- Raman	Calculated	Scaled			
51	-	-	450	432	6	3	ωCH(50)
52	-	-	411	396	3	4	tRasymd(48)
53	-	-	404	389	2	1	tRsymd(46)
54	-	335(vw)	351	338	1	5	tRtrigd(47)
55	-	-	332	320	6	5	tRasymd(45)
56	-	-	296	284	5	2	tRsymd(44)
57	-	-	244	234	3	2	tRtrigd(42)
58	-	-	219	211	4	0	bCCl(41)
59	-	-	182	175	1	3	ωCO(40)
60	-	-	158	152	0	0	ωCO(39)
61	-	-	151	145	0	0	ωCO(37)
62	-	-	147	141	1	2	ωCO(38)
63	-	-	114	109	4	0	ωCCl(36)
64	-	-	86	83	5	3	tCH_3(35)
65	-	-	66	63	2	2	tCH_3(34)
66	-	-	55	53	0	1	Butterfly(32)

Table 4 — Molecular orbital contributions of 4-Chloro-6,7-dimethoxyquinazoline

TD-DFT/ B3LYP/6-311++G(d,p)					Experimental wavelength (nm)
Energy (eV)	Oscillator strength	Computed wavelength (nm)	Major contributions	Assignment	
In gas phase					
4.0255	0.0033	308.00	H→L (85.23%)	π→π*	
4.1866	0.0715	296.15	H-2→L (85.95%)	π→π*	
4.4254	0.0222	280.16	H-1→L (61.66%)	π→π*	
In Water					330
4.0767	0.0815	304.13	H→L (88.75%)	π→π*	
4.1747	0.0056	296.99	H-2→L (90.029%)	π→π*	
4.3175	0.0602	287.17	H-1→L (74.45%)	π→π*	

produced with the B3LYP/6-311++G(d,p) technique differ just slightly. The frequencies of CH_3 ss are indicated by the Raman and CDQ FT-IR spectrum at 2970 and 2974 cm^{-1}, respectively. In the Raman and infrared spectrum, the symmetrical methyl deformation modes (CH_3 sb) are identified at 1413 cm^{-1} and 1385 cm^{-1}, respectively. Additionally, the Raman spectrum at 1435 and 1430 cm^{-1} shows that the methyl deformation modes are well-defined and mostly connected to in-plane bending vibrations, indicating the correlation with in-plane bending in CDQ. Using FT-IR, the out-of-plane stretching modes of CH_3 vibrations at 2902 and 2870 cm^{-1} are determined. For these assignments, literature supports the PED output. The calculated values exhibit good agreement with the Raman and infrared bands located at 1120 cm^{-1}, 1115 cm^{-1}, and 924 and 919 cm^{-1} in the spectrum. These bands are attribute to the in-plane and out-of-plane rocking modes of CH_3. Furthermore, the out-of-plane bending modes of CH_3 in CDQ are responsible for the bands observed at 1152 and 1130 cm^{-1} in the Raman and IR spectrum.

UV-visible and frontier molecular orbital analysis

In order to understand the electronic transitions of the molecule, electronic absorption spectrum were calculated using TD–DFT/B3LYP/6-311++G(d,p). The lowest singlet to singlet spin-allowed excited states of the title molecule have been considered. The calculation had been done for both the gas phase and the water solvent. The solvent effects must be taken into account because the spectrum data was analysed in water. The molecular orbital contribution of CDQ is summarised in (Table 4) together with the experimental absorption wavelengths. These values include absorption wavelengths (k), excitation energy (E), oscillator strengths (f), and the primary contributions of the transitions and assignments of electronic transitions. Along with the experimentally

obtained UV spectrum, the estimated electronic absorption UV spectrum in the gas phase and in water is displayed in (Fig. 5). The calculated absorption bands showed up in the gas phase at 308 nm (strong oscillator) and in water at 304.13 nm (strong oscillator), respectively. The primary electronic transition (85.23%) is from HOMO to LUMO, whereas HOMO-1 to LUMO (61.66%) is one of the smaller gas phase transitions. Comparably, in water, the primary electronic transition is from HOMO to LUMO (88.75%), whereas the minor transition is from HOMO-1 to LUMO (74.45%). The experimentally measured water spectrum, which likewise display an absorption band at 330 nm as seen in (Table 4), closely match the predicted absorption band at 304.13 nm. We consider only strong peak in experiment because other peaks have weak oscillator strength. The theoretical and experimental electronic absorption spectrum of the title molecule were found to be in good agreement.

Molecular orbital (MO) theory is the most frequently used theory in chemistry. Frontier molecular orbitals (FMOs) are used to estimate the interaction between different species. The two molecular orbitals that comprise the structure of the FMO: the lowest unoccupied molecular orbitals (LUMO) and the highest occupied molecular orbitals (HOMO). FMO evaluations provide important insights into the energy difference between HOMO and LUMO states. The CDQ compound were optimized using B3LYP functional with 6-311++G(d,p) basis set in both gas and water. The electrophile influences the LUMO state, the nucleophile contributes to the HOMO state. FMO can also be used to evaluate CDQ compound's stability. The energy gap between the HOMO and the LUMO plays an important role for charge transfer and biological activity within a molecule[31]. The positive phase (shown in red) and negative phase (shown in green) depict the charge transfer within the molecule as shown in (Fig. 6). From Figure 6, the HOMO and LUMO electrons are partially localized in quinazoline ring, chlorine and methyl group. A larger HOMO-LUMO gap indicates a hard molecule with high stability and low chemical reactivity, while a smaller gap indicates a soft molecule with less stability and high chemical reactivity. The computed energy gap values for the gas phase and water are 4.72 eV and 4.65 eV, respectively. The HOMO-LUMO plot for CDQ is given in (Fig. 6). According to Pauling, an atom's ability to attract electrons to itself within a compound is known as electronegativity. The HOMO and LUMO orbital energies, $I = -E_{HOMO}$ and $A = -E_{LUMO}$ represent ionisation energy and electron affinity, respectively. The term "electron affinity" indicates a ligand's capacity to receive exactly one electron from a donor. The negative electronegativity of a molecule is known as chemical potential (μ), which is approximately as $\mu = (E_{HOMO}+E_{LUMO})/2$. The global electrophilicity index (ω) ($\omega=\mu^2/2\eta$) measures the additional electronic charge that a molecule receives from its surroundings, causing its energy to stabilize. Low softness value (0.21) indicates the non-toxic nature of title compound. The chemical hardness of the compound is 2.35 eV and 2.32 eV for gas and water phases, respectively, confirming its stability. Additionally, the compound's ionization potential (which donates electrons) for gas phase and water is 7.03 eV, 7.04 eV and electron affinity (which accepts electrons) for gas phase and water is 2.31 eV, 2.39 eV are related to the HOMO and LUMO values. It must be noted that the organic molecules have higher ionization energy. Similar trend is observed in the present study also. The electrophilicity index for gas phase and water (4.63 eV and 4.79 eV) indicates the biological activity and supports molecular docking with various protein targets. Earlier Parthasarathi

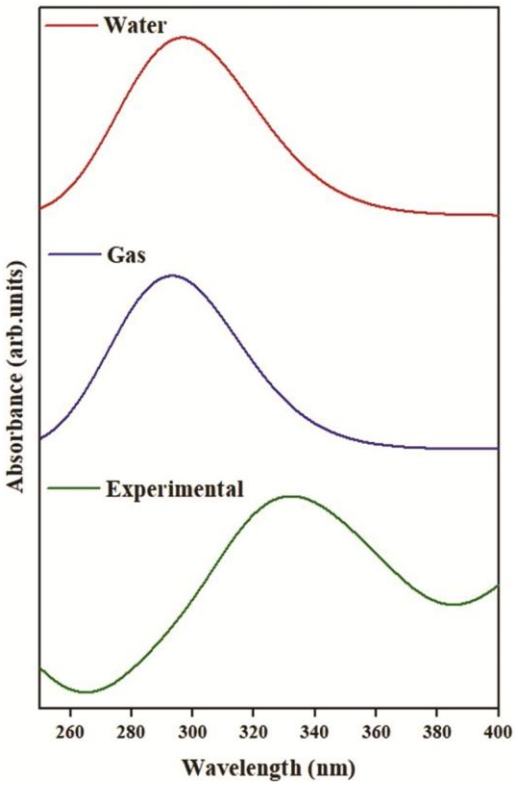

Fig. 5 — UV-Visspectrum of 4-Chloro-6,7-dimethoxyquinazoline

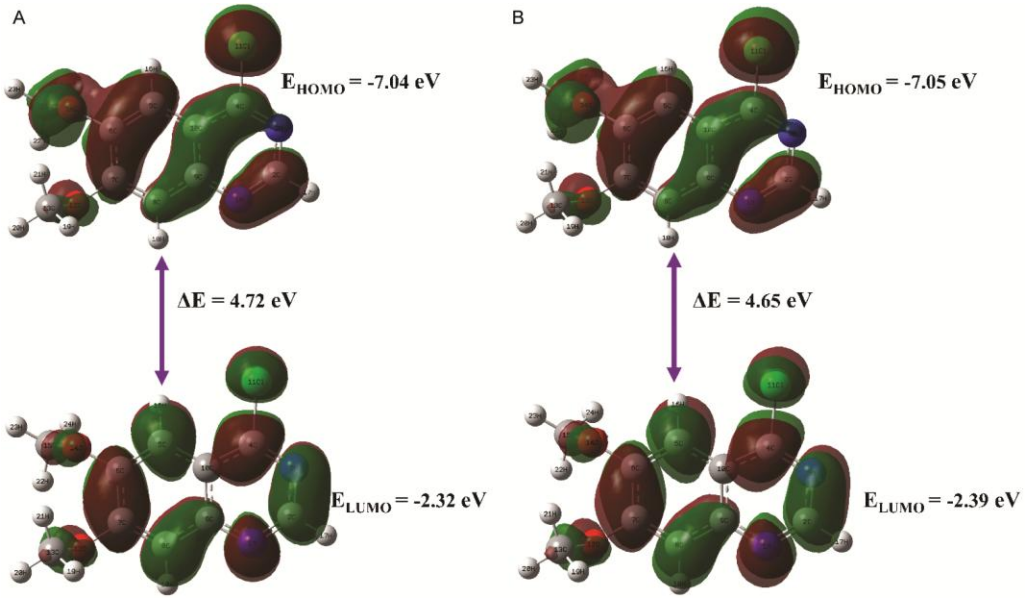

Fig. 6 — (A) gas phase; and (B) water of HOMO-LUMO plot for 4-Chloro-6,7-dimethoxyquinazoline

Table 5 — Global reactivity descriptors for 4-Chloro-6,7-dimethoxyquinazoline

Molecular Properties	B3LYP/6-311++G(d,p)	
	In gas phase	In Water
HOMO (eV)	-7.03	-7.04
LUMO (eV)	-2.31	-2.39
ΔE (E_{HOMO} -E_{LUMO}) (eV)	4.72	4.65
Ionization potential (I) (eV)	7.03	7.04
Electron affinity (A) (eV)	2.31	2.39
Global hardness (η) (eV)	2.35	2.32
Global softness (S) (eV^{-1})	0.21	0.21
Electronegativity (χ) (eV)	4.67	4.72
Chemical potential (μ) (eV)	-4.67	-4.72
Global electrophilicity (ω) (eV)	4.63	4.79

et al. have demonstrated the suitability of electrophilicity index to describe biological activity[32]. The electronegativity of the chemical is defined as its ability to attract shared electrons, and it is found to be 4.67 eV for gas phase and 4.72 eV for water. The calculated CDQ values of the global reactivity descriptors are shown in the (Table 5).

Molecular electrostatic potential

Molecular electrostatic potential (MEP) study identifies reactive sites and establishes physic-chemical relationships between compounds. Protons are projected *via* electrons and neutrons using an electric charge cloud to depict the MEP. It shows positive, negative, and neutral electrostatic areas using colour grading and relative polarity of molecules. These surfaces also show the charge density, molecular structure, size, and chemical reactivity sites of molecules. Additionally, MEP provides adequate information for identifying regions involving intra- and intermolecular interactions[33]. The distinct electrostatic potential regions represented by the various colours on the molecule's MEP surface are as follows. Light blue is slightly electron deficient; yellow is slightly electron rich; green is neutral; red is electron rich with a partially negative charge; and blue is electron deficient with a partially positive charge. The MEP of CDQ, which were calculated using the B3LYP/6-311++G(d,p) method, had been plotted in (Fig. 7) and visualised using the Gauss View 5.0 program for gas phase and water using colour grading.In the gas and water phases, compound color varies from -7.568 e^{-2} to 7.568 e^{-2} and -7.658 e^{-2} to 7.658 e^{-2}. The electron-deficient blue regions are primarily found over the electron-donating methyl group (CH_3), contributing to nucleophilic reactivity. The red electronegative (electron-rich) regions are predominantly situated over the N1 and N3 atoms in the pyrimidine ring, which are responsible for electrophilic attacks. The green regions, indicating neutrality, that are mainly located over the Cl atom.

Mulliken population analysis

The Mulliken charges contributed to atoms vibrational characteristics significantly. Additionally, they identified which atom is positively charged and which is negatively charged. It identified which atom was slightly an electron donor or acceptor during bond formation. So, this may have influenced the

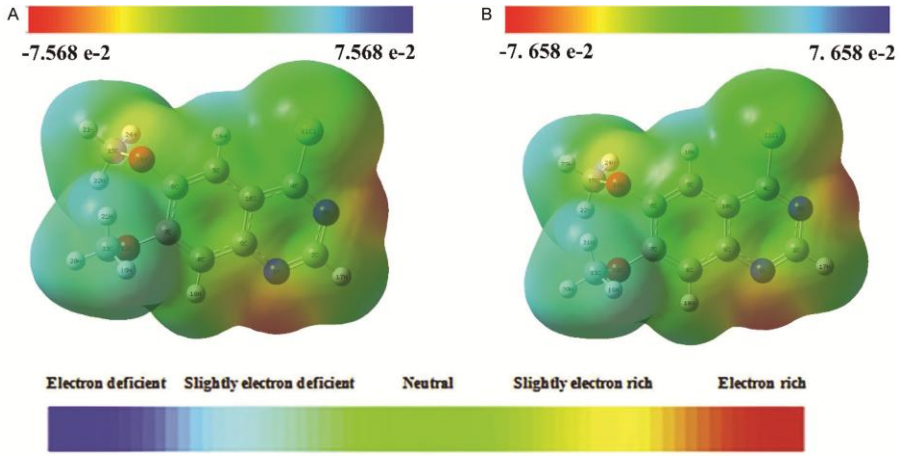

Fig. 7 — (A) gas phase; and (B) water of MEP plot for 4-Chloro-6,7-dimethoxyquinazoline

dipole moment and polarizability of the molecule[34]. Mulliken population study is used to investigate many aspects of molecular structure by giving each atom in the molecule a distinct charge. In this study, CDQ have been calculated using DFT / B3LYP with 6-311++G(d,p) basis set for gas phase and water. The results were shown in (Suppl. Table 1 and Fig. 8). The mulliken charges plot for CDQ is given in (Fig. 8). Interestingly, Figure8 shows that electronegative elements like N, O, and Cl have more positive charges or less negative charges. For instance, N1 atom in the pyrimidine ring has positive charge as well as nearby C2 has negative charge and C9 atoms have positive charges. C10 atom has more positive charge, this is due to nearby C atoms in the benzene ring. These atoms possess less positive or negative charges. Every hydrogen atom has a positive charge since they all have the ability to donate electrons to nearby carbon atoms. In CDQ, an electronegative atom is surrounded with carbon atoms, and any C atom is surrounded by electronegative atoms. All of the CDQ atoms mulliken atomic charges are displayed in (Suppl. Table 1). It is evident from (Fig. 8 and Suppl. Table 1) that there is a significant charge transfer between the C atoms and the electronegative atoms. This large charge transfer will affect the reactivity sites. That is these electron rich sites favourable for electrophilic attack. Methyl group attached with the pyrimidine ring is favourable for nucleophilic attack. However, because of their electron localisations, electronegative elements are generally more susceptible to electrophilic attack. For further, clarification NBO charges are used to study the reactivity study. The results show good correlation with one another and with MEP findings. A wide

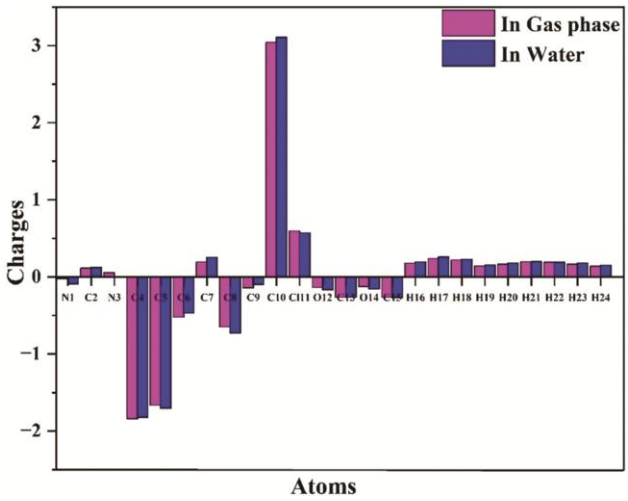

Fig. 8 — Mulliken charges plot for 4-Chloro-6, 7-dimethoxyquinazoline

range of chemical systems reactive behaviour in both electrophilic and nucleophilic reactions can be interpreted and predicted using the mulliken population method and MEP.

Natural bonding orbital analysis

By using natural hybrid and atomic orbitals, natural bond orbitals (NBO) are produced from the input atomic orbital basis set. The Gaussian output file specifies the standard orientation of the system, which is aligned with the NBO analysis results. Second-order perturbation theory have been used to study all possible interactions between filled (donor) Lewis-type NBOs and empty (acceptor) non-Lewis NBOs. We calculate the delocalisation stabilisation energy E (2) for every acceptor NBO (j) and donor NBO (i). The NBO analysis of the CDQ molecule is performed by applying the DFT/B3LYP/6-311++G(d,p) approach.

Comparing "filled" (donors) Lewis-type NBOs with "empty" (acceptors) non-Lewis NBOs, (Suppl. Table 2) shows the second-order perturbation energy values, E (2)ij. The orbitals in CDQ that have the highest stabilization energies are π(C5-C6)→π*(C7–C8), π(C5-C6)→π*(C9-C10), π(C7–C8)→π*(C5–C6), π(C7–C8)→π*(C9–C10), π(C9–C10)→π*(C5–C6), and π(C9–C10)→π*(C7–C8) (17.62, 16.01, 16.8, 18.28, 17.59, and 14.03 kcal mol^{-1}). All of these orbitals have the highest stabilization energies. These interactions result in high electron concentrations (about 0.27e and 0.47e) in the anti-bonding acceptor C–C orbitals. Supplementary Table S2 is a list of the factors that heavily impact the stability of the CDQ molecule.

Topology studies

LOL and ELF

The localized orbital locator (LOL), represented by η(r), and the electron localization function (ELF), represented by τ (r), were subjected to topological analysis using the Multiwfn program[35]. That are widely used to classify chemical bonds, and show how the atomic shell is structured, and confirm charge-shift bonds on the surface of molecules. Electron kinetic energy in ELF is closely related to electron repulsion and offers a localized measure of it. Greater values of ELF (0.0 to 1.0) show that electrons are highly localized, indicating the presence of inner shells, a lone pair of atoms, or a covalent connection. Lower values (<0.5) depict places where electrons are likely to be delocalized. The color grade shown in the LOL and ELF maps verify the presence of bonding and nonbonding electrons. Figure 9A & B provide a projected plot of ELF and LOL. When the red color value is at its maximum, it means that there are electrons surrounding the hydrogen atoms and methyl group, (CH_3) that are both bonding and nonbonding. In Figure 9A, the blue color cloud surrounding the carbon and chlorine atoms indicates low electron localization values. The carbon, nitrogen, oxygen, and chlorine atoms are surrounded by little blue rings that demonstrate the extent of electron depletion that takes place between the inner shell and valence. The red color suggests that they are present in close proximity to hydrogen atoms with high LOL values due to covalent interactions between the atoms. As shown in Figure 9B, electron density is the reason for the hydrogen atoms with a maximum range encircled by tiny white circles.

Reduced density gradient (RDG), Non-covalent interaction (NCI)

RDG analysis is a visual technique that gives non-covalent interactions in molecular systems more accuracy and used to examine intra- and inter-non-bonded interactions[36]. The RDG have been calculated using quantum mechanical methods like DFT and visualised as a three-dimensional map to depict electron density distribution in space. The CDQ molecule's RDG scatter graphs and gradient

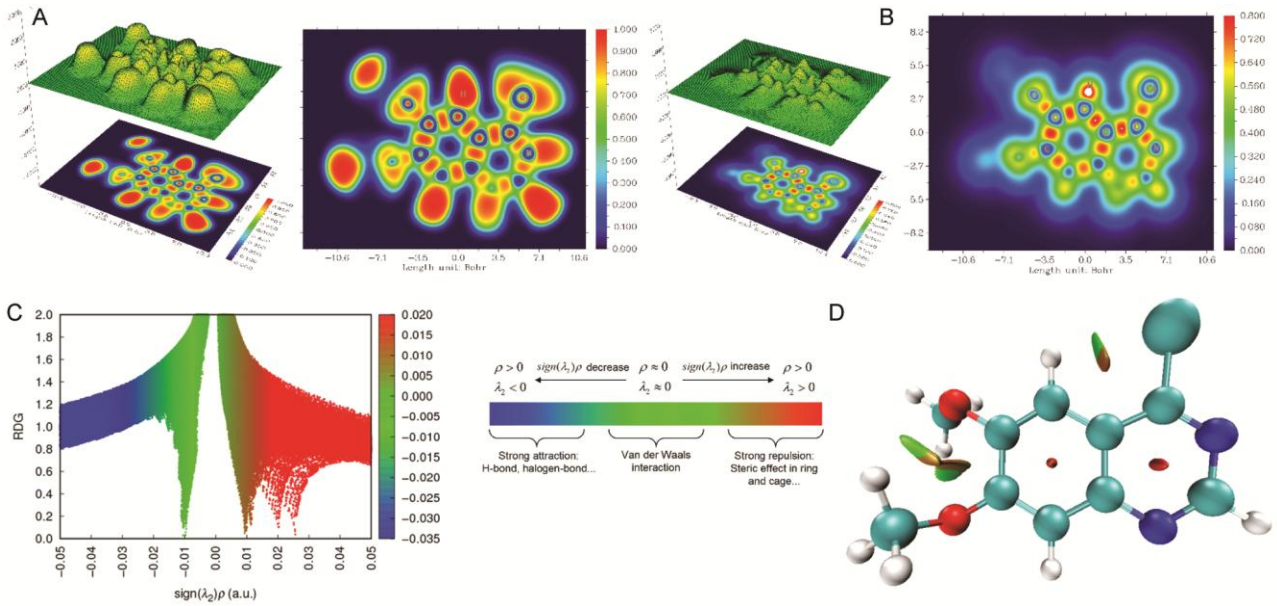

Fig. 9 — (A) Projected ELF plot; (B) Projected LOL plot; (C) Scattered RDG plot; and (D) 3d non-covalent interaction plot of 4-Chloro-6,7-dimethoxyquinazoline

isosurfaces have been shown in (Fig. 9C). Plotting RDG against sign (λ2)ρ, where sign(λ2)ρ is the second eigenvalue of the electron density, results in an RDG scatter graph. This value provides significant information on the type and intensity of interactions. The sign and value of sign (λ2)ρ can be used to identify the type of interaction. sign (λ2)ρ < 0 indicates an attractive interaction, sign (λ2)ρ almost zero indicates a Vanderwaals interaction, and sign (λ2)ρ > 0 indicates an repulsive interaction[37]. The three colors that make up the RDG scatter spectrum are red, green, and blue. λ2(r) has a function that varies from -0.035 to 0.020 a.u.The steric repulsion is shown by the red spike in the RDG isosurfaces. The RDG scatter plot shows the red contour between 0.02 and 0.05 a.u, which indicates the larger repulsive exchange contribution. On the RDG scatter graph, a blue contour that falls between -0.02 and -0.05 a.u. denotes strong hydrogen bonding. The vander Wals interaction is indicated by the red-green mixed flaky area between 0.01 and -0.015 a.u, which also illustrates the lack of hydrogen bonding. This information is verified by the title compound's two-dimensional scatter plot. The Multiwfn software was used to create the RDG scatter diagram, which was then displayed on an EPS viewer.

We can determine the noncovalent interaction (NCI) of the title compound by analysing the non-covalent index using electron density (ρ), its derivative (∇ρ), and the Laplacian ($\nabla^2\rho$). The 3d NCI (Non-covalent interaction) plot of the CDQ is shown in (Fig. 9D). Hydrogen bonding shows important attraction at ρ>0 and λ2<0 conditions. The strong hydrogen bonding interaction takes place between two methyl (CH_3) group, (H22-H21) and C112-H18. The CDQ exhibits two repulsive effects. Both of them are placed inside the benzene ring.

Molecular docking

Molecular docking is a simulation tool used for drug discovery to anticipate the binding mechanism and affinity of small molecules to a target macromolecule. Molecular docking predicts optimal ligand position and conformation within the macromolecule's binding site. Algorithms used in these programs explore through millions of ligand orientations and conformations to determine the most beneficial for energy binding posture. Molecular docking simulations assess large chemical libraries to identify prospective therapeutic candidates and improve binding affinity through structure-based drug design. The main aim of Molecular dockingis: (i) Identify the ligand-receptor binding mode with the lowest binding energy score; and (ii) calculate thebinding affinity of the interaction. This crucial data can be used to develop new drugs and gain insights into the mechanisms of ligand-receptor interactions. To understand the patterns of interaction between the four proteins (4EY7, 1EVE, 4PQE and 3I6M) and CDQ, a docking study was carried out. The CASTp server was used to find out the binding pocket in the selected proteins[38].

Using Pyrx software, the CDQ molecule was further docked with protein. Based on their hydrogen/hydrophobic interactions and lowest binding energy, the docked molecules have been evaluated. The docked molecules optimum position has been identified using the lowest binding energy. The calculated binding affinity for all targeted proteins (4EY7= -7.5 kcal mol^{-1}, 1EVE= -7.4 kcal mol^{-1}, 4PQE= -7.4 kcal mol^{-1}, 3I6M= -7.0 kcal mol^{-1}) are given in (Table 6). CDQ interacts with 4EY7 protein and shows three interactions. Hydrogen bond interactions such as TYR A341, HIS A447, SER A203 with a distance of 2.27,2.49, 2.79 Å. Attractive charge and Pi-sigma interactions also takes place such as TYR A337 (3.89 Å), ASP A74 (4.59 Å) and TYR A86 (3.94 Å) and PHE A338 (3.89 Å). The 3D and 2D interactions of CDQ-4EY7 plots are shown in (Fig. 10A). Similarly, CDQ interacts with 1EVE protein forming a stable complex establishing one hydrogen bond HIS A440 with a distance of 2.25 Å. The other interactions such as attractive charge and Pi-cation ASP A72 (4.53 Å), PHE A330 (3.65 Å), TYR A334 (4.90 Å), TRP A84 (4.05 Å), and Pi-sigma interaction such as PHE A331 (3.92 Å). Therefore, the smallest distance has strong binding energy. The 3D and 2D interactions of CDQ-1EVE complex are shown in (Fig. 10B). CDQ interacts with 4PQE has one hydrogen bond interaction TYR A124 at 1.86 Å distance. Carbon hydrogen bond interaction takes place at THR A83 (3.56 Å). Attractive charge and

Table 6 — Calculated binding affinity (kcal mol^{-1}) of 4-Chloro-6,7-dimethoxyquinazoline against target proteins using PyRx

Protein Name	PDB ID	Binding affinity
Recombinant Human Acetylcholinesterase	4EY7	-7.5
ARICEPT	1EVE	-7.4
Human Acetylcholinesterase	4PQE	-7.4
Torpedo californica acetylcholinesterase	3I6M	-7.0

Pi-sigma interactions also takes place such as GLU A202 (4.57 Å), TRP A86 (4.59 Å) and TYR A337 (3.92 Å). The 3D and 2D interactions of CDQ-4PQE plots are shown in (Fig. 10C). Finally, CDQ interacts with 3I6M protein and has two carbon hydrogen bond interaction HIS A440 with a distance of 3.35 Å and SER A200 (3.51 Å). Other interaction has same as 1EVE protein interaction but small variation in distance. Attractive charge and Pi-cation ASP A72 (4.35 Å), PHE A330 (3.99 Å), TYR A334 (2.73 Å), and Pi-sigma interaction such as PHE A331 (3.83 Å). The 3D and 2D interactions of CDQ-3I6M plots are shown in (Fig.10D). In all four-protein, hydrogen bond interaction takes place in oxygen atom due to methyl group attached on it. Hence it is concluded that 4EY7 protein has lowest binding energy (-7.5 kcal mol^{-1})compared to other proteins. As a result, the CDQ ligand has the strongest interaction with Alzheimer proteins and may be able to reduce their activity of AD.

Molecular dynamics

Protein-ligand complexes were analysed using MD simulations to verify their stability. GROMACS was employed to analyze the stability of protein-ligand complexes over a 25 ns time period. We used MD simulations in order to study the docked complexes of the PDB, 4EY7 with CDQ. The docking result indicates that the protein 4EY7 with CDQ has strong binding energy (-7.5 kcal mol^{-1}).The system had been solvated using the SPC water model in a 2.0 nm cubic box with two chlorine ions added to neutralise it.

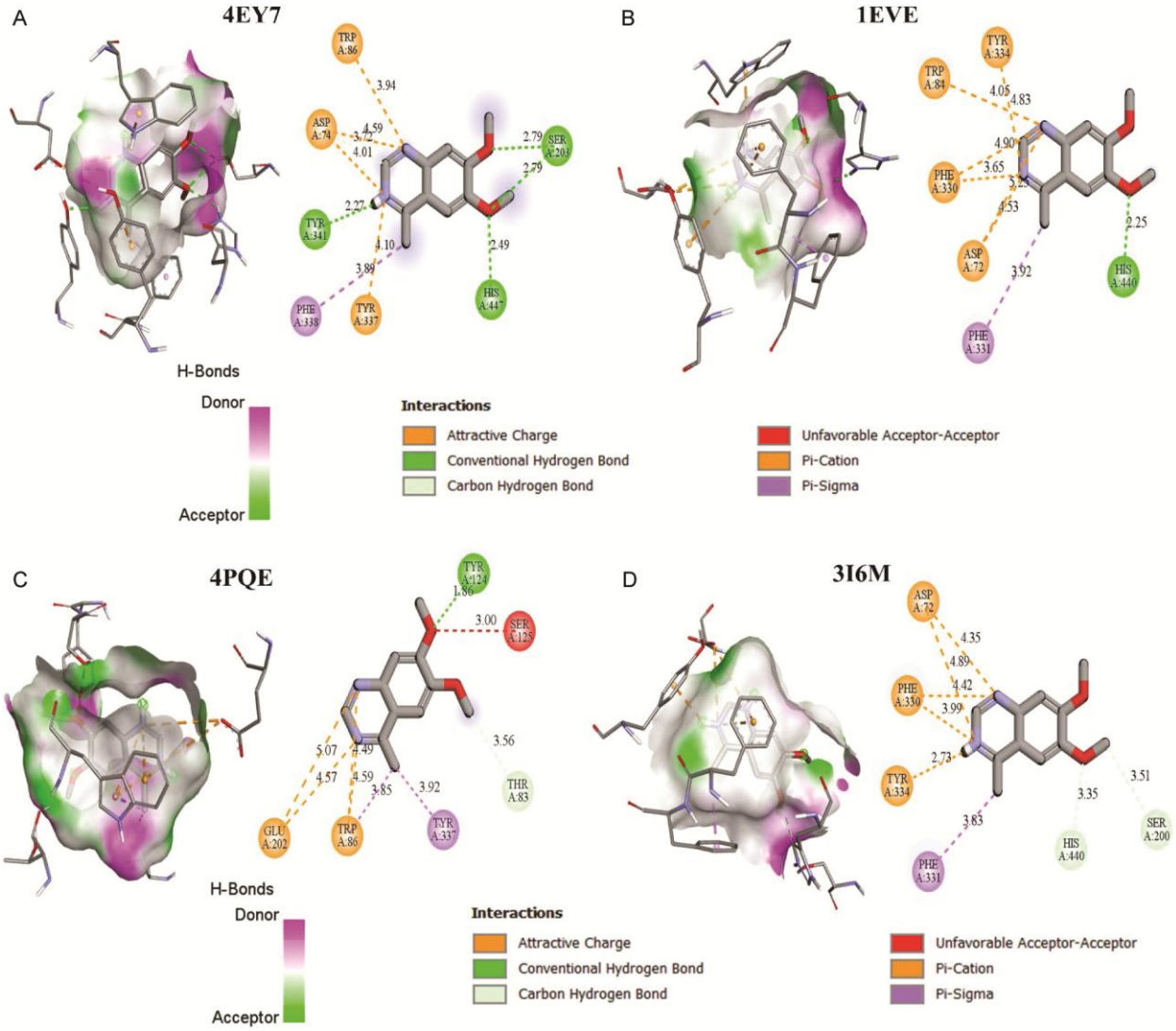

Fig. 10 — 3D and 2D interaction with H-Bond donor-acceptor colour grade of 4-Chloro-6,7-dimethoxyquinazoline molecule with target protein

Distinct boundary conditions were applied in all directions. During the system's setup, 50,000 steepest descending steps were selected to minimise energy and avoid any unfavourable encounters. The technique of changing atom positions to obtain the system's most stable configuration is known as energy minimisation. The Van der Waals and electrostatic interaction ensembles were equilibrated using the Parrinello-Rahman coupling method. The temperature and pressure coupling constants have been set to 0.1 ps and 1, respectively, to create a stable environment of 300 K temperature and 1 bar pressure. In order to calculate long-range electrostatic interactions, MD simulations were run over a 25-ns period at constant pressure using the NPT ensemble. The compound was neutralised, and it most likely contained the model protein. Neutralization involves adding counterions to a system to balance its charge and achieve electrical neutral. During a 25 ns period, the compound was dynamically modelled, with ongoing updates to atom velocities and positions to analyze the system's dynamic behavior.

GROMACS was used to analyse the simulation trajectory and determine parameters such as RMSD (Root Mean Square Deviation), RMSF (Root Mean Square Fluctuation), number of hydrogen bonds formed inside the compound and radius of gyration (R_g). These investigations provided insights into the simulated system's stability, flexibility, and intermolecular interactions. In MD simulation, the RMSD method can be used to calculate the average distance generated by atom displacement over a given time frame compared to a reference time frame. The RMSF must be used to identify and describe local conformational changes in both the protein chain and the ligands employed. By measuring the alpha-carbon atoms RMSF and the protein's backbone's RMSD throughout the period of 25 ns MD trajectories, conformational changes in proteins and their stability were examined. Figure 11 shows an MD analysis of the lead compound. The backbone RMSDs of protein ligand complexes (Fig. 11A) were analysed throughout a 25 ns simulation period to assess their

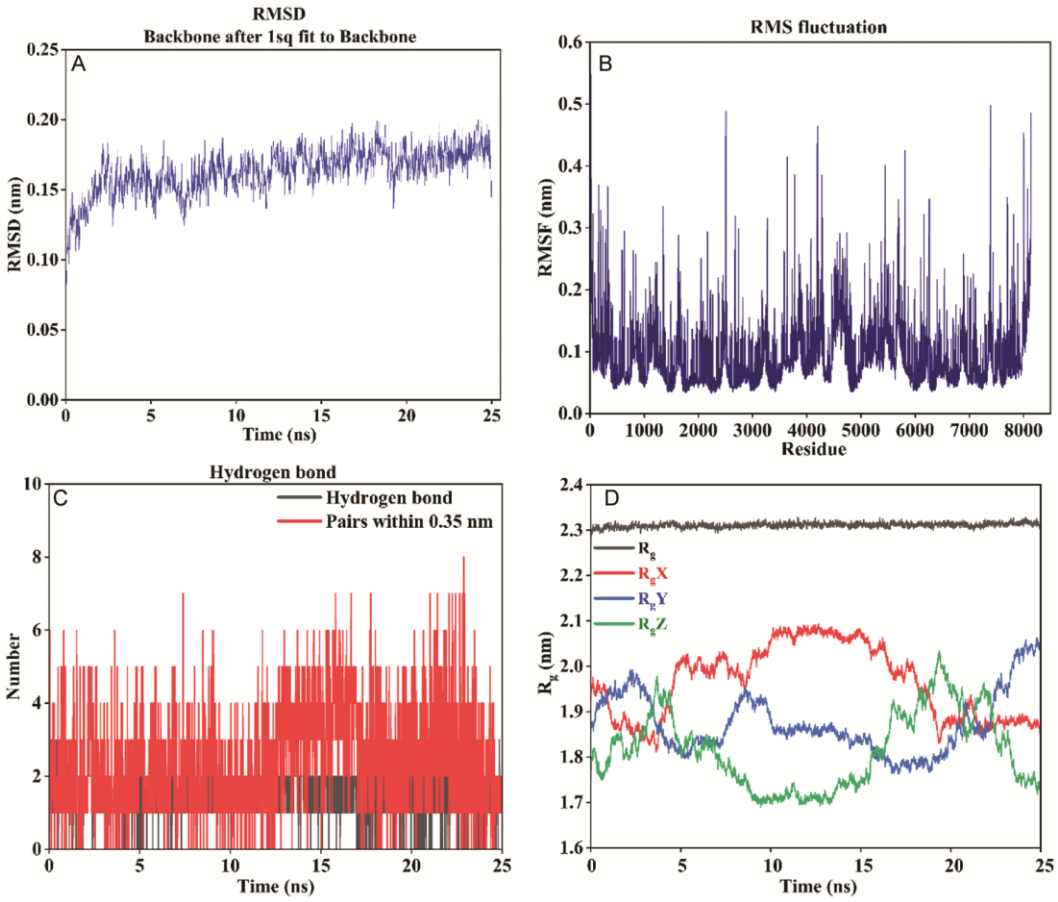

Fig. 11 — Molecular dynamics analysis of (A) Root mean square deviation (RMSD); (B) Root mean square fluctuation (RMSF); (C) Hydrogen bond; and (D) Radius of gyration (R_g) of 4-Chloro-6,7-dimethoxyquinazoline

structure and dynamic properties. The RMSD of 4EY7-CDQ was observed at a very small deviation at 0.18 nm from 0 to 9ns and it was stabilized after 18ns throughout the simulation period. RMSF is a key statistic that provides information about each residue's structural flexibility. The RMSF of the protein-ligand complex (Fig. 11B) indicated a minimized fluctuation of 0.49 nm at 2508residues. Throughout the 25-ns simulation period, the RMSF remained relatively stable, suggesting minimal impact on the compound's stability. Polar interactions between proteins and ligands significantly influence their binding affinity. Conventional hydrogen bonds between the protein and ligand contribute to the stabilization of the complex. The MD simulation results indicate that the number of hydrogen bonds (Fig.11C) formed between CDQ and the 4EY7 active site varied from zero to three during the 25 ns simulation. To fully understand the nature and importance of these interactions, more investigation is required. The radius of gyration (R_g) parameter, depicts the protein structure's size and conformational changes during the MD simulation, may not adequately capture the structural changes at the molecular level. The R_g values for the protein (R_g X), the protein-ligand complex (R_g Y), and the ligand (R_g Z) showed minimal variations throughout the simulation, suggesting only slight structural changes. The R_g values were 1.95 nm for the protein, 1.85 nm for the protein-ligand complex, and 1.8 nm for the ligand, as shown in (Fig.11D). These detailed evaluations suggest that CDQ is a highly reliable and stable candidate. Because of its compact R_g values, little RMSF fluctuations, low RMSD, and hydrogen bonding interactions, and it is a promising candidate for the development of an anti-Alzheimer's drug.

ADMET and physicochemical properties

The ADMET characteristics serve an important purpose. The ADMET studies are carried out using pkSCM online server. Caco-2 cell culture is the most used *in vitro* model to investigate drug permeability in oral medications. According to the pkCSM server measurement, a log Papp value more than 0.90 indicates higher levels of Caco-2 permeability[39]. CDQ has a log Papp of 1.365 (in 10^{-6} cm/s), indicating that it is highly permeable to Caco-2. When a molecule is delivered orally in the body excellent absorption is a desirable quality. The human intestine plays a crucial role in the absorption of nutrients and pharmaceutical compounds. Compounds with an absorption rate of less than 30% are regarded as poor intestinal absorption[40]. The intestinal absorption rate of CDQ in humans is 96.22%. The oral administration of a drug with a higher HIA may enhance intestinal absorption. The primary problems in the creation of topical drugs are breaking through the skin's protective layer. Several *in silico* methods have been used to predict the skin penetration of the synthesised drug molecule. pkCSM server data suggest that CDQ contributed to higher dermal permeability, with a log Kp value of -2.344. The term "hypothetical volume of distribution" (VDss) indicates that the drug is uniformly dispersed to achieve a concentration that is comparable to blood plasma. Greater VDss indicates that the drug has been distributed more widely in tissue than in plasma. A molecule's absorption and distribution throughout the system were determined by the combination of lipophilic and hydrophilic groups in the structure. According to pkCSM server, a large volume of distribution as log VDss >0.45 (VDss >2.81 L/kg), whereas a low volume of distribution is represented by VDss in log VDss >0.15 (VDss >0.71 L/kg).CDQ has a VDss of -0.456 (log L/kg), demonstrating a huge amount of dispersal. The Blood-Brain Barrier (BBB) serves as a permeable shield to protect the brain from harmful chemicals. A molecule mayeasily penetrate the BBB if its logBB is greater than 0.3; a logBB of -1, shows that the molecule is poorly distributed to the brain[41]. The pkCSM server shows a significant distribution of CDQ to the brain, as indicated by logBB = 0.418. CNS (Central Nervous System) permeability (logPS) is another straight-forward assessment performed using in situ brain insertion, with the drug administered directly into the carotid artery. The pkCSM prediction system considers compounds with logPS > -2 as capable of penetrating the CNS, while those with logPS < -3 are deemed incapable. CDQ has a logPS value of -2.317, indicating its ability to penetrate the central nervous system. This study also predicted the inhibitory activity of P-glycoprotein (P-gP) and cytochrome P450, two key factors in metabolism. Cytochrome P450 (CYP), the body's primary detoxification enzyme, plays a crucial role in pharmaceutical metabolism. Cytochrome P450 exists in the following isoforms: CYP1A2, CYP3A4, CYP2C9, CYP2C19, CYP2D6, and CYP2E1. At doses lower than 10 mM, the cytochrome P450 inhibitor can inhibit the enzyme by 50%. Moreover, CYP2D6 and CYP3A4 are significant contributors to drug metabolism. However,

CDQ does not effectively inhibit most cytochrome P450 isoforms. The inhibition and activation of P-glycoprotein (P-gP) significantly impact drug metabolic pathways. According to pharmacokinetic predictions, CDQ does not affect P-glycoprotein activity. The pkCSM server indicates that CDQ has a total clearance rate of 0.64 as a renal OCT2 substrate. Evaluation of pharmacokinetic properties has shown that CDQ, as a ligand molecule, satisfies most of the requirements for drug-likeness, which makes it an appropriate choice for treating AD.

Predicting a compound's toxicities is a crucial step in the development of new drugs. A molecule's toxicity profile is important, and the CDQ molecule exhibits no Ames toxicity, indicating that it might not be carcinogenic. Skin sensitivity is a latent dermally applied drugs; so, CDQ does not possess skin sensitivity. The maximum tolerated dose of CDQ in humans was determined as 0.733 log mg/kg/day. Oral CDQ treatment in rats was shown to have acute and chronic toxicity limits of 2.644 mol/kg (LD_{50}) and 1.762 log mg/kg_bw/day (LOAEL). In addition to being quicker, *in silico* toxicity evaluations have the potential to minimize the number of animal trials. So, we calculated LD_{50} values for the compound. The LD50 value is the number of doses required to kill 50% of a test population, such as lab rats or other animals. The lower the LD_{50} dose, the higher the toxicity of the drug. The CDQ compound shows higher LD_{50} (2.644) value and has less toxicity. The pkCSM server reports that CDQ does not inhibit hERG I or II. Table 7 shows the predicted Pharmacokinetic parameters of CDQ.

Physicochemical properties

Determining the physicochemical properties of the compounds have been the main objective. SwissADME is a free online tool for evaluating the drug-likeness, lipophilicity, solubility, and Boiled Egg Model of the lead chemical CDQ, as shown in the (Table 8). The lead compound CDQ has a molecular weight of 224.64 g/mol and no violations, based on the results from SwissADME. The CDQ lead compound has just four hydrogen bond acceptors and zero hydrogen bond donor. A drugs solubility and degree of aliphaticity can be assessed using the fraction of sp-3 carbon atoms in the molecule. For the drug compound under investigation, Fraction sp-3 carbon was found to be 0.2. The molar refractivity and topological polar surface area (TPSA) for CDQ compound is 57.53 and 44.24. In the study, the

Table 7 — Predicted pharmacokinetic parameters of 4-Chloro-6,7-dimethoxyquinazoline molecule using pkCSM server

Property	Parameters	Predicted Value
	Water Solubility	-2.571 (log mol/L)
	CaCo-2 permeability	1.365 (log Papp in 10^{-6} cm/s)
	Intestinal absorption	96.22%
Absorption	Skin Permeability	-2.344 (log Kp)
	P-glycoprotein Substrate	No
	P-glycoprotein I inhibitor	No
	P-glycoprotein II inhibitor	No
	VDss (human)	-0.456 (log L/kg)
Distribution	Fraction unbound (human)	0.279 (Fu)
	BBB permeability	0.418 (log BB)
	CNS permeability	-2.317 (log PS)
	CYP2D6 substrate	No
	CYP3A4 substrate	No
	CYP1A2 inhibitior	No
Metabolism	CYP2C19 inhibitior	No
	CYP2C9 inhibitior	No
	CYP2D6 inhibitior	No
	CYP3A4 inhibitior	No
Excretion	Total Clearance	0.64
	Renal OCT2 substrate	No
	AMES toxicity	No
	Max. tolerated dose (human)	0.733 (log mg/kg/day)
	hERG I inhibitor	No
	hERG II inhibitor	No
Toxicity	Oral Rat Acute Toxicity (LD50)	2.644 (mol/kg)
	Oral Rat Chronic Toxicity (LOAEL)	1.762 (log mg/kg_bw/day)
	Hepatotoxicity	Yes
	Skin Sensitisation	No
	T.Pyriformis toxicity	0.704 (log ug/L)
	Minnow toxicity	0.687 (log mM)

Table 8 — Predicted physicochemical parameters of 4-chloro-6,7-dimethoxyquinazoline molecule using SwissADME tool

Properties	Parameters	Values
Physiochemical properties	Molecular weight (g/mol)	224.64
	No. of Hydrogen bond acceptors	4
	No. of Hydrogen bond donors	0
	Fraction Csp	0.2
	Molar refractivity	57.53
	TPSA (A^2)	44.24
Water Solubility	ESOL	-3.13
	ALI	-3.01
	SILICOS	-4.21

(*Contd*.)

Table 8 — Predicted physicochemical parameters of 4-chloro-6,7-dimethoxyquinazoline molecule using SwissADME tool (*Contd*.)

Properties	Parameters	Values
Lipophilicity	iLOGP	2.41
	XLOGP3	2.44
	WLOGP	2.30
	MLOGP	1.26
	SILICOS-IT	2.53
Drug Likeness	Lipinski	Yes 0 violation
	Veber	Yes 0 violation
	Ghose	Yes 0 violation
	Egan	Yes 0 violation
	Bioavailability Score	0.55
	Synthetic accessibility	1.76

lipophilicity of iLOGP, XLOGP3, WLOGP, MLOGP, and SILICOS-IT was estimated to be 2.41, 2.44, 2.30, 1.26 and 2.53. The CDQ water solubility ESOL, ALI, and SILICOS-IT were estimated to be -3.13, -3.01, and -4.21, respectively. Water solubility results vary from very soluble to moderately soluble. The CDQ compound has no violations and complies with all regulations (Lipinski, Veber, Ghose, and Egan).The bioavailability score ranges from 0 to 1, for our compound it is 0.55.We determined the synthetic accessibility (SA) score of drug-like compounds on a scale of 1 (extremely simple) to 10 (very difficult)[42].For our compound the synthetic accessibility score is 1.76. Based on these predicted Physicochemical properties, CDQ is found to be a nontoxic drugs candidate that has not violated any of the other criteria. Table 8 shows the Predicted physicochemical parameters of CDQ.

The following standards have been used in order to calculate the drug-likeness assessment scores: GPCR ligand, ion channel modulator, kinase inhibitor, nuclear receptor ligand, protease inhibitor, and enzyme inhibitor. A bioactivity score falls into one of three categories: inactive if it is less than -5.0, moderately active if it is between -5.0 and 0.0, and active if it is greater than 0[43]. The compound was found to be moderately bioactive for GPCR ligand (-0.39), ion channel modulator (-0.12), kinase inhibitor (-0.02), nuclear receptor ligand (-0.73), protease inhibitor (-0.88) and enzyme inhibitor (-0.06). Table 9 represent the Drug-likeness assessment of CDQ.

Egg model

Blood-brain barrier (BBB) penetration and Gastrointestinal (GI) absorption are essential steps in the drug development process. The BOILED-Egg plot is useful for calculating polarity and lipophilicity of

Table 9 — Drug-likeness assessment of 4-Chloro-6, 7-dimethoxyquinazoline by Molinspiration

Bioactivity	Values
GPCR ligand	-0.39
Ion channel modulator	-0.12
Kinase inhibitor	-0.02
Nuclear receptor ligand	-0.73
Protease inhibitor	-0.88
Enzyme inhibitor	-0.06

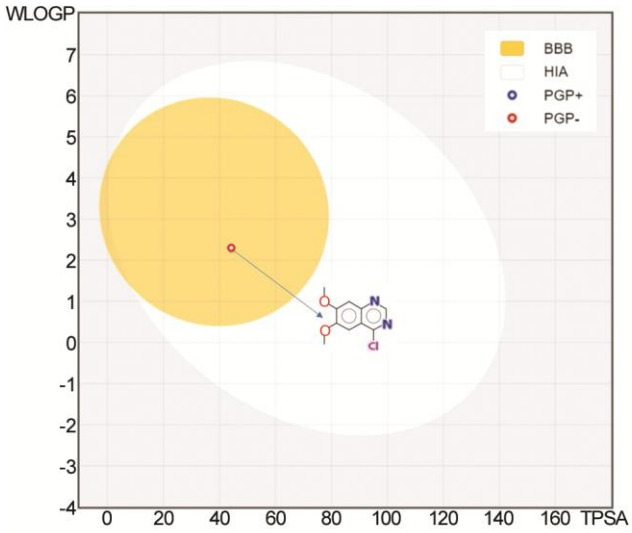

Fig. 12 — BOILED-Egg plot for 4-Chloro-6, 7-dimethoxyquinazoline

derivatives, that provide accurate, fast and clear graphical results[44]. The method screens chemical libraries to aid in drugs development. In the BOILED-Egg plot, as shown in (Fig. 12), the yellow portion (yolk) denotes substantial BBB penetration, whereas the white region reflects passive GI tract absorption. The BOILED Egg model of CDQ shows that the drugs ingredient penetrates the BBB and emerges within the yolk section. In addition, the blue color indicates that the molecule is actively effused by P-gP (PGP^+), whereas the red colour indicates that the molecule is not a substrate for P-gp (PGP^-).

Conclusion

In this work, the experimental and computational methods were used to quantify the extensive spectroscopic investigations on CDQ. All DFT calculation have been performed using B3LYP/6-311++G(d,p) level of theory. The optimised geometrical parameters show good agreement with the experimental results. The thermodynamical parameters such as entropy, enthalpy, and heat capacity have been used to confirm the thermal

stability of the compound under investigation. The experimentally measured water spectrum wavelength (330 nm) matches with computed wavelength (304.13 nm). The molecule's stability and bioactive characteristics have been confirmed by the computed HOMO and LUMO energy gap (4.72 eV for gas phase and 4.65 eV for water). The global reactivity characteristics of the molecule were used to identify reactive sites in CDQ. MEP and Mulliken charge analyses shows that electrophilic and nucleophilic chemical reactivity sites. The hyper-conjugative relationship between charge delocalisation and molecular stability have been investigated through NBO analysis. Identification of strong and weak hydrogen bonds is made easier by topological analysis of atoms within a molecule. Using RDG plot surface analysis, the interactions that take place within the molecule (the steric effect and the Van der Walls interaction) are analysed. Molecular docking and other *in silico* techniques were employed to investigate the inhibitory properties against AD. With values ranging from -7.5 kcal/mol^{-1} to -7.0 kcal/mol^{-1}, CDQ demonstrated a good binding affinity with 4EY7 protein. Furthermore, our molecular dynamics simulations demonstrate that CDQ maintains a stable structure and is well aligned with the target protein, increasing its potential as a candidate for AD.Finally, the physicochemical and ADMET properties confirm CDQ's drug-like characteristics, indicating that it is nontoxic and adheres to Lipinski's guidelines. However, additional *in vitro* and *in vivo* studies are necessary to validate our conclusions. The findings of the current study may assist medicinal and pharmaceutical chemists in developing and synthesizing more potent candidates for anti-Alzheimer drugs. Consequently, ongoing research is paving the way for the development of novel drugs to treat AD.

Acknowledgement

K.A. is thankful to the management of Kalasalingam Academy of Research and Education for the university research fellowship.

Conflict of interest

All authors declare no conflicts of interest.

References

1 Knopman DS, Amieva H, Petersen RC, Chételat G, Holtzman DM, Hyman BT, Nixon RA& Jones DT, Alzheimer disease. *Nat Rev Dis Prim*, 7 (2021) 33.

2 Nichols E, Steinmetz JD, Vollset SE, Fukutaki K, Chalek J & Abd-Allah F, Estimation of the global prevalence of dementia in 2019 and forecasted prevalence in 2050: an analysis for the Global Burden of Disease Study 2019. *Lancet Public Heal*, 7 (2022) 105.

3 Çakmak Ş & Erdoğan T, Some bis (3-(4-nitrophenyl) acrylamide derivatives: Synthesis, characterization, DFT, antioxidant, antimicrobial properties, molecular docking and molecular dynamics simulation studies. *Indian J Biochem Biophys*, 60 (2023) 209.

4 Selkoe DJ & Hardy J, The amyloid hypothesis of Alzheimer's disease at 25 years. *EMBO Mol Med*, 8 (2016) 595.

5 Kametani F & Hasegawa M, Reconsideration of amyloid hypothesis and tau hypothesis in Alzheimer's disease. *Front Neurosci*, 12 (2018) 328460.

6 Francis PT, Palmer AM, Snape M & Wilcock GK, The cholinergic hypothesis of Alzheimer's disease: a review of progress. *J Neurol Neurosurg Psychiatry*, 66 (1999) 137.

7 Padurariu M, Ciobica A, Lefter R, Serban IL, Stefanescu C & Chirita R, The oxidative stress hypothesis in Alzheimer's disease. *Psychiatr Danub*, 25 (2013) 401.

8 Jabir NR, Khan FR & Tabrez S, Cholinesterase targeting by polyphenols: A therapeutic approach for the treatment of Alzheimer's disease. *CNS Neurosci Ther*, 24 (2018) 753.

9 Bilginer S, Gul HI, Anil B, Demir Y & Gulcin I, Synthesis and *in silico* studies of triazene-substituted sulfamerazine derivatives as acetylcholinesterase and carbonic anhydrases inhibitors. *Arch Pharm (Weinheim)*, 354 (2021) 2000243.

10 Asokan K & Paranthaman S, Investigation of cholinergic inhibition by donepezil-rimegepant hybrids in alzheimer's disease: An in silico study. *Indian J Biochem Biophys*, 61 (2024) 788.

11 Vaz M & Silvestre S, Alzheimer's disease: Recent treatment strategies. *Eur J Pharmacol*, 887 (2020) 173554.

12 Bajad NG, Singh RB, Gajendra TA, Gutti G, Kumar A, Krishnamurthy S & Gopichand G, Development of multi-targetable chalcone derivatives bearing N-aryl piperazine moiety for the treatment of Alzheimer's disease. *Bioorg Chem*, 143 (2024) 107082.

13 Matilda JJ & Abbs Fen Reji TF, Design, structural characte rization, biological evaluation and molecular doocking studies of fmethylinndole bearring thiocaarbamoylppyrazole moieties. *Indian J Biochem Biophys*, 61 (2024) 418.

14 Rehuman NA, Al-Sehemi AG, Parambi DGT, Rangarajan TM, Nicolotti O, Kim H & Bijo M, Current progress in quinazoline derivatives as acetylcholinesterase and monoamine oxidase inhibitors. *ChemistrySelect*, 6 (2021) 7162.

15 Rohini R, Reddy PM, Shanker K, Hu A & Ravinder V, Antimicrobial study of newly synthesized 6-substituted indolo [1, 2-c] quinazolines. *Eur J Med Chem*, 45 (2010) 1200.

16 Vasdev N, Dorff PN, Gibbs AR, Nandanan E, Reid LM, O'Neil JP & Henry FV, Synthesis of 6-acrylamido-4-(2-[18F] fluoroanilino) quinazoline: a prospective irreversible EGFR binding probe. *J Label Compd Radiopharm Off J Int Isot Soc*, 48 (2005) 109.

17 Saravanan G, Alagarsamy V & Prakash CR, Synthesis and evaluation of antioxidant activities of novel quinazoline derivatives. *Int J Pharm Pharm Sci*, 2 (2010) 83.

18 Kunduracioglu A, A Computational (DFT) Study on the Anti-Malarial Drug: Lumefantrine. *Appl Sci*, 13 (2023) 9219.

19 Anigboro AA, Avwioroko OJ, Akeghware O & Tonukari NJ, Anti-obesity, antioxidant and in silico evaluation of Justicia carnea bioactive compounds as potential inhibitors of an enzyme linked with obesity: Insights from kinetics, semi-empirical quantum mechanics and molecular docking analysis. *Biophys Chem*, 274 (2021)106607.

20 Alvarado M, Barceló M, Carro L, Masaguer CF & Raviña E, Synthesis and biological evaluation of new quinazoline and cinnoline derivatives as potential atypical antipsychotics. *Chem Biodivers*, 3 (2006) 106–117.

21 Malamas MS & Millen J, Quinazolineacetic acids and related analogs as aldose reductase inhibitors. *J Med Chem*, 34 (1991) 1492.

22 Frisch M, gaussian 09, Revision d. 01, Gaussian. *Inc, Wallingford CT*, 201 (2009).

23 Dennington R, Keith T, Millam J & others, GaussView, version 5, (2009).

24 Noury S, Colonna F, Savin A & Silvi B, Analysis of the delocalization in the topological theory of chemical bond. *J Mol Struct*, 450 (1998) 59.

25 Goel S & Kumar Y, Assessing Inhibitory potential of natural compounds against BACE1 in Alzheimer's disease: A molecular docking and molecular dynamics simulation approach. *Indian J Biochem Biophys*, 61 (2024) 345.

26 Biovia DS, Discovery studio modeling environment. Release, (2017).

27 Dallakyan S & Olson AJ, Small-molecule library screening by docking with PyRx. *Methods Mol Biol*, 1263 (2015) 243.

28 Lai CP, Bo L & Huang SD, 4-amino-2-chloro-6, 7-dimethoxyquinazoline methanol solvate. *Acta Crystallogr Sect C Cryst Struct Commun*, 53 (1997) 906.

29 Şahin ZS, Kantar GK, Şaşmaz S & Büyükgüngör O, Synthesis, molecular structure, spectroscopic analysis, thermodynamic parameters and molecular modeling studies of (2-methoxyphenyl)oxalate. *J Mol Struct*, 1087 (2015) 104.

30 Jamróz MH, Vibrational energy distribution analysis (VEDA): scopes and limitations. *Spectrochim Acta Part A Mol Biomol Spectrosc*, 114 (2013) 220.

31 Karthik N, Jeyavijayan S & Sumathi S, Docking studies, molecular structure, and spectroscopic analysis of 3-chlorobenzamide as an anti-cancer agent. *Indian J Biochem Biophys* , 61 (2024) 204.

32 Parthasarathi R, Subramanian V, Roy DR & Chattaraj PK, Electrophilicity index as a possible descriptor of biological activity. *Bioorg Med Chem*, 12 (2004) 5533.

33 kumar JS, Karthik N, Sumathi S, Jyothi NS, Saranya S, & Jeyavijayan S, DFT Computation, Spectroscopic, Hirshfeld Surface, Docking and Topological Analysis on 2,2,5-Trimethyl-1,3-Dioxane-5-Carboxylic Acid as Potent Anti-Cancer Agent. *Int J Quantum Chem*, 124 (2024) 27509.

34 Ghosh K, Roy S, Ghosh A, Banerjee A, Bauzá A, Frontera A & Chattopadhyay S, Three mononuclear octahedral cobalt (III) complexes with salicylaldimine Schiff bases: Synthesis, characterization, phenoxazinone synthase mimicking activity and DFT study on supramolecular interactions. *Polyhedron*, 112 (2016) 6.

35 Lu T & Chen F, Multiwfn: A multifunctional wavefunction analyzer. *J Comput Chem*, 33 (2012) 580.

36 Contreras-García J, Boto RA, Izquierdo-Ruiz F, Reva I, Woller T & Alonso M, A benchmark for the non-covalent interaction (NCI) index or is it really all in the geometry. *Theor Chem Acc*, 135 (2016) 1.

37 Jia Z, Pang H, Li H & Wang X, A density functional theory study on complexation processes and intermolecular interactions of triptycene-derived oxacalixarenes. *Theor Chem Acc*, 138 (2019) 1.

38 Pulakuntla S, Singh SA, Kuruvalli G, Shaik AH & Reddy VD, Molecular docking and dynamics analysis to reveal the therapeutic potential of Dostarlimab against novel immune targets in liver cancer. *Indian J Biochem Biophys*, 61 (2024) 740.

39 Kunjumol VS, Karthik N, Sumathi S & Jeyavijayan S, Spectroscopic, computational, docking, and cytotoxicity studies on 5-chlorobenzimidazole as a Potent anti-breast cancer agent. *Indian J Biochem Biophys*, 61 (2024) 804.

40 Pires DE V, Blundell TL & Ascher DB, pkCSM: Predicting Small-Molecule Pharmacokinetic and Toxicity Properties Using Graph-Based Signatures. *J Med Chem*, 58 (2015) 4066.

41 Sukumaran S, Zochedh A, Viswanathan TM, Sultan AB, & Kathiresan T, Theoretical investigation of 5-fluorouracil and tamoxifen complex–structural, spectrum, DFT, ADMET and docking simulation. *Polycycl Aromat Compd*, 43 (2023) 9443.

42 Shadrack DM & Ndesendo VMK, Molecular docking and ADMET study of emodin derivatives as anticancer inhibitors of NAT2, COX2 and TOP1 enzymes. *Comput Mol Biosci*, 7 (2017) 1.

43 Suganya M, JoseKavitha S & Rajakannan V, *Insilico* Studies of Molecular Property and Bioactivity of Organic Crystalline Compounds using Molinspiration. *Int Res J Eng Technol*, 7 (2020) 5193.

44 Daina A & Zoete V, A boiled-egg to predict gastrointestinal absorption and brain penetration of small molecules. *ChemMedChem*, 11 (2016) 1117.